A Kinetic Blueprint for Bioactive Ceramics: Programming the Bio-interface through Thermal Processing

Andualem Belachew WORKIE, Department of Materials Science and Engineering, National Taiwan University of Science and Technology, Taipei, Taiwan, and Shao-Ju SHIH, Department of Materials Science and Engineering, National Taiwan University of Science and Technology, Taipei, Taiwan.
E-mail: andualembelachew2@gmail.com and girum569@gmail.com

Abstract

The therapeutic performance of a bioactive ceramic is dictated not by its static bulk properties, but by the dynamic evolution of its bio-interface over time. However, predicting and controlling this temporal cascade remains a major challenge. Here, we establish a kinetic blueprint for apatite-wollastonite glass-ceramics (A-W GCs) by programming their initial phase composition through controlled sintering (700–1100°C). We then systematically tracked the subsequent bio-interfacial cascade in simulated body fluid (SBF), quantifying ion exchange kinetics, surface biomineralization, and material degradation. Our findings demonstrate a direct link between the initial phase composition and the material's bioactivity profile. Specifically, A-W GCs sintered at 1100°C, rich in crystalline wollastonite, exhibited controlled ion release and served as a superior template for rapid, uniform hydroxyapatite (HA) layer formation. In contrast, lower-temperature, amorphous-rich samples displayed rapid, uncontrolled dissolution and poor subsequent mineralization. This study demonstrates that the entire therapeutic lifecycle of a bioceramic, from initial ionic signaling to final surface maturation, can be precisely programmed through a single fabrication variable. This approach redefines biomaterial design by focusing on engineering the timing of biological responses, rather than just mimicking composition. It lays the foundation for developing advanced, smart materials with controllable and predictable therapeutic outcomes.

Keywords: Bioactive Ceramics, Apatite-Wollastonite Glass-Ceramic, Sintering, Templated Biomineralization, Interfacial Engineering, Hydroxyapatite

1. Introduction

Long-term success of orthopedic and dental implants depends on their capacity to create a solid and functional contact with host tissue [1, 2] . Apatite-wollastonite glass-ceramics (A-W GCs) are one type of bioactive material that is specifically made for this use. Bioactive ceramics actively interact with the physiological environment, triggering a series of actions that result in direct bone apposition, in contrast to bio-inert materials that induce a fibrotic capsule [3-5]. This therapeutic effect is the consequence of a dynamic, time-dependent process that takes place at the material-biofluid interface rather than an inherent characteristic of the bulk material itself [6, 7].

Ion exchange and partial dissolution are the results of the material surface's initial interaction with biofluids, which is a well-postulated sequence of processes. The local chemical microenvironment is altered as a result, and biophysical cues are then provided for the nucleation and formation of a new, biologically recognized mineral layer, usually hydroxyapatite (HA) substituted with carbonate [8, 9]. Tissue integration begins when cells detect and react to this freshly produced layer. Therefore, the main objective of logical biomaterial design is to comprehend and regulate the

kinetics of this dynamic biophysical dialogue, from the initial ion flux to the presentation of a mature, cell-adhesive topography.

Although our earlier research developed a reliable technique for regulating the first phase composition of A-W GCs via thermal sintering and spray pyrolysis [10, 11], the critical link between this initial state and the subsequent kinetic cascade remains unquantified. This research attempts to close that gap. We speculate that we can predictably program the spatiotemporal evolution of the bio-interface and, consequently, the final biological response of the material by carefully engineering the early phase assemblage (the surface). By methodically monitoring the important kinetic processes, such as ion exchange, pH modulation, surface mineralization, and matrix degradation, for A-W GCs with different starting compositions, we dissect this process and create a fundamental, biophysically based model.

However, this static design philosophy largely overlooks the critical role of temporal kinetics. The biological response is not instantaneous; it is a dynamic cascade of events unfolding over time. A critical limitation in the field is the lack of a predictive framework to control this kinetic sequence. Therefore, a shift is needed from designing materials with a desired final composition to programming materials with a predictable, time-dependent therapeutic trajectory.

In this work, a comprehensive process-structure-property-performance (PSPP) link is established for the first time in this system. Sintering determines phase assembly, which in turn determines the kinetic cascade and final bio-functionality.

2. Materials and Methods

2.1 Synthesis of Homogeneous Glass-Ceramic Precursors

To achieve chemical homogeneity, a precursor powder representing the A-W GC system was produced in order to explicitly examine the impact of thermal processing on phase transitions. 4.6 MgO, 44.7 CaO, 34.0 SiO_2, 16.2 P_2O_5, and 0.5 CaF_2 were the goal composition (wt.%) that was attained by a spray pyrolysis process that used continuous aerosol generation. Tetraethyl orthosilicate (TEOS, 98.0%, Thermo Scientific), calcium nitrate tetrahydrate (CNT, 98.5%, Showa), magnesium nitrate hexahydrate (MgN, 99.0%, Acros Organics), triethyl phosphate (TEP, 99.0%, Thermo Scientific), and calcium fluoride (CaF_2, 99.0%, Sigma Aldrich) were used to prepare an aqueous solution. This method was adapted from previous protocols [10].

An ultrasonic nebulizer operating at 1.65 MHz was used to atomize the solution into tiny aerosol droplets. A vertically aligned three-zone quartz tube furnace carried the droplets via carrier gas. To help with precursor breakdown and in-flight calcination, the zones were kept at 700°C and 250°C, respectively, to evaporate the solvent. Phase segregation, which is frequently linked to conventional batch synthesis, was successfully reduced by this efficient thermal technique, which produced an ultrafine, amorphous-rich powder with remarkable compositional consistency at the nanoscale.

2.2 Engineering the Initial Surface State via Controlled Sintering

The as-synthesized precursor powder was uniaxially crushed into cylindrical pellets 10 mm in diameter at 60 MPa to serve as substrates for the kinetic analysis. To produce a systematic change in the initial material surface condition, these pellets were treated to a well-regulated thermal treatment regimen. Using a programmable air furnace, samples were heated at a steady rate of 5°C/min to one of five discrete peak sintering temperatures: 700, 800, 900, 1000, or 1100°C. Each temperature was kept for four hours to allow the system to attain thermodynamic equilibrium before being cooled in the furnace. This procedure generated five distinct sets of A-W GCs, each with its own well-defined beginning phase assembly and microstructure, which served as the study's independent variable. The phase composition of these non-immersed samples was assessed using Rietveld refinement of x-ray diffraction (XRD) data as the baseline (t=0) for the kinetic study.

2.3 Simulating the Bio-interfacial Cascade: A Time-Resolved Immersion Study

To study the spatiotemporal evolution of the surface-interface-response cascade, five sets of sintered pellets were immersed in acellular Simulated body fluid (SBF). The SBF was generated with ion concentrations almost equivalent to those of human blood plasma, following the published methodology of Kokubo et al. [12]. The immersion was carried out under dynamic settings in a shaking water bath with a constant physiological temperature of 37°C to simulate the body's environment. All samples had a standardized surface area-to-volume ratio (S_a/V) of 0.1 cm^{-1}. The study included discrete points for investigation at t = 3, 5, 7, 14, and 21 days to capture both the quick early events and the interface's long-term maturity.

2.4 Spatiotemporal Deconstruction of the Kinetic Cascade

A multi-modal analytical procedure was run at each time point to determine the kinetics of the bioactive cascade. This strategy was developed to decouple the interconnected events at the material-biofluid interface by systematically probing three distinct but concurrent aspects of the system's evolution: (i) the interfacial chemical environment, (ii) surface structural transformation, and (iii) net macroscopic degradation.

2.4.1 Chemical Kinetics: Interfacial pH Profiling

To determine the kinetics of the initial biophysical trigger, the pH of the SBF solution was profiled at each time point. Using a calibrated pH meter (PH500, CLEAN), this measurement provided a sensitive real-time proxy for the net ion flux at the ceramic-fluid interface. The obtained kinetic profiles offered quantitative information about the rate and degree of the surface-driven chemical modulation that starts the bioactive cascade.

2.4.2 Probing Interfacial Structural Evolution and Mineralization Kinetics

Following immersion, the structural evolution of the pellet surfaces was studied at the micro- and nanoscales. The surface topography and coalescence of the new mineral layer were observed using Field Emission Scanning Electron Microscopy (JEOL JSM-6500F). Surface-sensitive X-ray diffraction (Bruker D2 Phaser, Cu Kα radiation) was used to quantify the crystallographic change. XRD patterns were utilized to establish the identity of the precipitated phase

(hydroxylapatite) and to monitor the attenuation of initial matrix phases (wollastonite), providing quantitative kinetic data on the biomineralization process.

2.4.3 Macroscopic Kinetics: Gravimetric Degradation Profiling

To determine the overall kinetic outcome of the bioactive cascade, the material's bulk degradation was profiled using a gravimetric technique. The dry weight of the pellets (sintered at 1100°C and selected for their excellent bioactivity) was measured before immersion (W_0) and after immersion and drying at each time point (W_t). The accumulated weight loss percentage was computed as: $Weight\ Loss\ (\%) = [(W_0 - W_t)/W_0] \times 100$. This generated kinetic data about the material's bulk degradation and resorption potential

3. Results

3.1 Sintering Temperature Dictates Initial Phase Composition and pH Response

The initial phase composition of the A-W GCs was directly controlled by the sintering temperature. As shown by XRD analysis (Figure 1A), samples sintered at 700–800°C were predominantly amorphous, while samples heated to 1100°C became progressively crystalline, showing a high abundance of the wollastonite phase.

Upon immersion in SBF, the initial phase composition dictated the kinetic response at the interface. Samples rich in amorphous phases (700-800°C) induced a rapid and significant increase in the pH of the SBF. In contrast, the crystalline, wollastonite-rich sample (1100°C) produced a muted but stable pH profile that remained within the 7.46-7.58 range (Figure 1B).

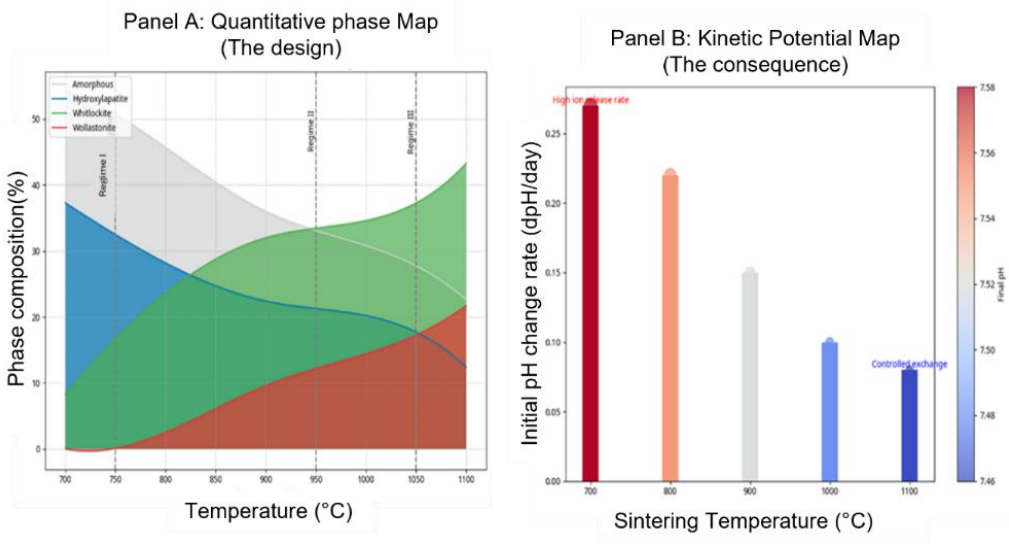

Figure 1. Engineered surface states and biophysical potential. (A) Phase composition evolution with sintering temperature, showing crystallization regimes. (B) Kinetic behavior in SBF

3.2 Interfacial Structural Evolution and Mineralization Kinetics

The evolution of the surface structure was monitored over 21 days. Scanning electron microscope (SEM) imaging revealed a stark contrast in mineralization potential based on the initial surface state (Figure 2). The wollastonite-rich

1100°C sample exhibited the nucleation of a new mineral layer by day 7, which coalesced into a dense, widespread, and mature crystalline layer by day 21. Conversely, the amorphous-rich 700°C sample showed only sparse and insufficient mineralization even after 21 days.

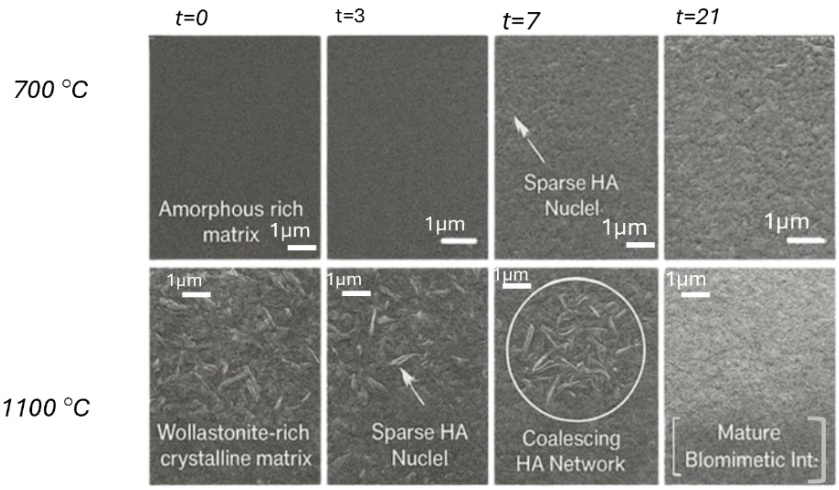

Figure 2. SEM timeline comparing interfacial structure evolution at 700°C (top) and 1100°C (bottom) over 3, 7, and 21 days. The wollastonite-rich 1100°C surface accelerates and enhances HA layer development.

This structural transformation was quantified using XRD (Figure 3A). For the 1100°C sample, immersion in SBF for 21 days resulted in a dramatic attenuation of the primary wollastonite peaks and the appearance of new, intensified peaks identified as HA. The kinetic transformation over time (Figure 3B) shows an inverse relationship: as the normalized intensity of the HA phase increased, the intensity of the wollastonite phase decreased in a corresponding manner.

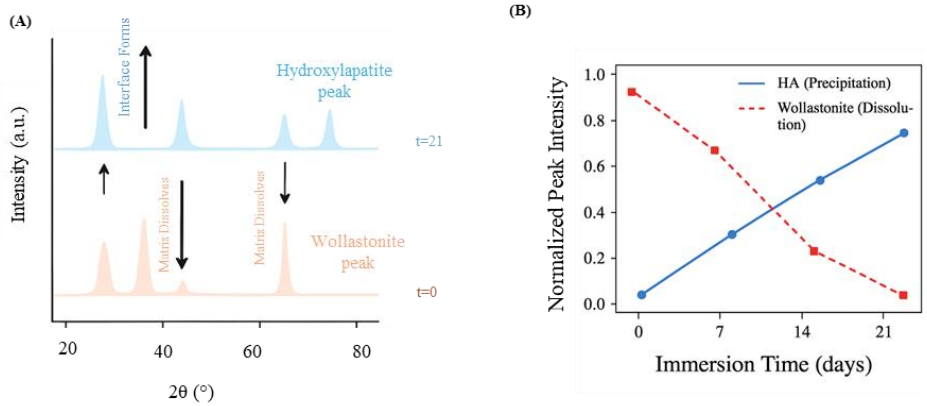

Figure 3. Dissolution–Reprecipitation kinetics at the 1100°C A-W GC interface. (A) XRD patterns at t = 0 and 21 days show a marked decrease in Wollastonite peaks alongside intensified signals from newly formed HA. (B) Normalized peak intensities linking Wollastonite dissolution to HA interface growth.

3.3 Macroscopic Degradation Profile

The net material response was quantified by gravimetric analysis of the 1100°C sample. The material exhibited a regulated, non-linear degradation profile (Figure 4). The instantaneous degradation rate was high initially and decreased progressively over the 21-day immersion period. This resulted in a total accumulated weight loss of approximately 2.5%.

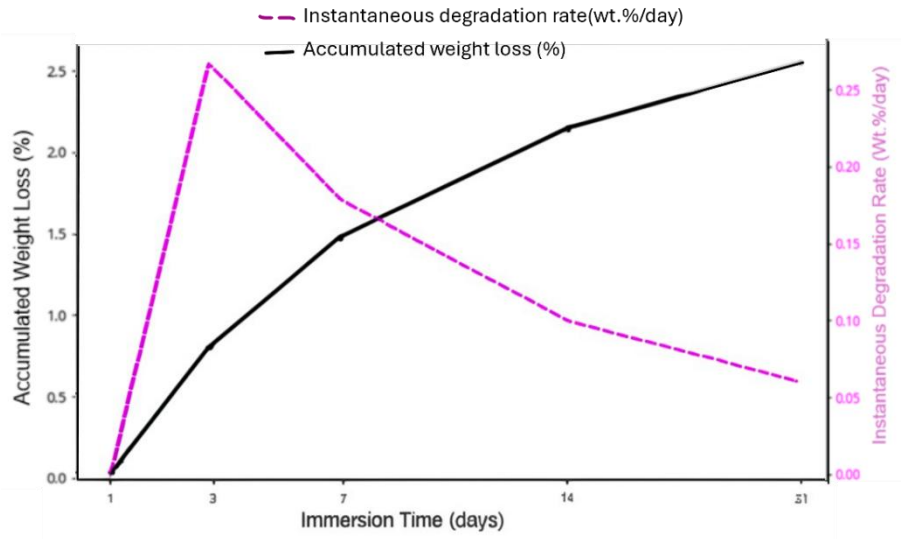

Figure 4 Non-linear degradation of the 1100°C sample, driven by time-dependent formation of a bioactive HA layer that regulates progressive weight loss.

3.4 A Unified Model of the Bioactive Cascade

To synthesize these interconnected findings, a conceptual model was developed to illustrate the complete kinetic blueprint from initial material design to final therapeutic outcome, as presented in Figure 5.

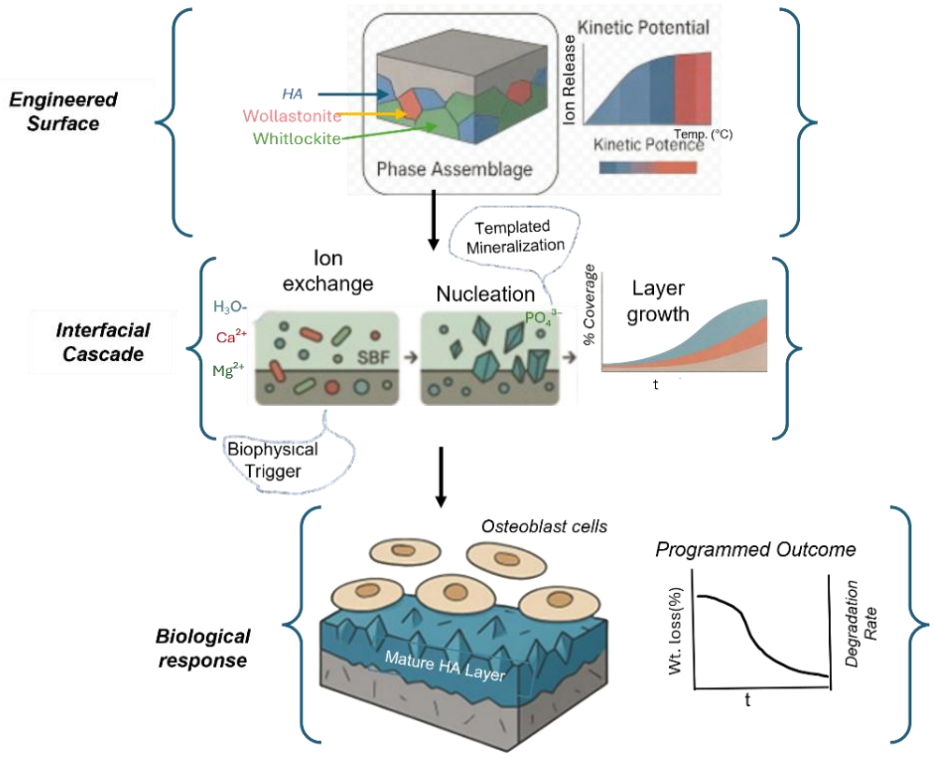

Figure 5. Schematic of a unified kinetic bioactivity model, linking surface composition, interfacial evolution, and downstream therapeutic response, offering a blueprint for time-programmed bioactive material design.

4. Discussion

This study successfully demonstrates that the bio-interfacial cascade of A-W glass-ceramics can be predictably programmed by engineering the initial phase composition via thermal processing. Our results show a clear link between the initial surface state and the subsequent kinetic sequence of ion exchange, biomineralization, and material degradation.

The first biophysical cue is the immediate ion exchange upon implantation. The rapid pH increase observed for the amorphous-rich samples (700–800°C) can be attributed to their higher Gibbs free energy compared to their crystalline counterparts, which drives a strong chemical potential gradient and rapid dissolution. While this initiates a chemical signal, it is largely uncontrolled. In contrast, the more crystalline, the wollastonite-rich sample (1100°C) exhibited a more regulated ion exchange. This muted but stable pH modulation is therapeutically significant, as it maintains the local environment within the optimal osteogenic window (pH 7.46-7.58) and releases a controlled flux of ionic signaling molecules (Ca^{2+}, Mg^{2+}, and silicates) known to influence gene expression and angiogenesis [13, 14].

The controlled release of specific ions from the 1100°C A-W GC surface does more than just modulate local pH; it represents a sophisticated form of biological signaling. This elevates the role of ion exchange from a simple chemical consequence to a crucial therapeutic mechanism. Extracellular calcium ions (Ca^{2+}) are well-known second messengers that can directly activate cell-surface receptors, such as the calcium-sensing receptor (CaSR), which is expressed on osteoblasts and their precursors [15]. Activation of the CaSR is known to initiate intracellular signaling cascades,

including the mitogen-activated protein kinase (MAPK) pathway, which in turn promotes osteoblast proliferation and differentiation. Furthermore, the dissolution products of silicate-based ceramics, primarily in the form of orthosilicic acid ($Si(OH)_4$), have been shown to be potent biological regulators. At the genetic level, silicon has been demonstrated to upregulate the expression of key osteogenic genes, including collagen type I, which forms the primary organic scaffold of bone, and critical differentiation markers like Runx2 and Osterix [16]. Therefore, the programmed, stable release of both Ca^{2+} and silicate ions from the wollastonite-rich surface provides a sustained set of instructive cues, creating a microenvironment that is actively pro-osteogenic rather than merely permissive.

This initial chemical shift dictates the second stage: templated biomineralization. The superior performance of the 1100°C sample in forming a dense HA layer is not random precipitation. It is a direct consequence of its wollastonite-rich surface chemistry acting as a template. The breakdown of the wollastonite phase exposes a high density of Si-OH groups, which are negatively charged at physiological pH and attract Ca^{2+} ions from the SBF. This localized concentration of critical ions lowers the interfacial energy barrier (ΔG^*) for heterogeneous nucleation, making the formation of stable apatite nuclei both thermodynamically and kinetically favorable [9]. The inverse relationship between the dissolution of the wollastonite matrix and the precipitation of the HA layer (Figure 3B) provides clear, quantitative evidence for this coupled dissolution-reprecipitation mechanism.

It is instructive to contrast the direct templating mechanism observed in our wollastonite-rich system with the canonical bioactivity pathways of other well-known materials. The classical mechanism for melt-derived 45S5 Bioglass®, for instance, involves a more complex, five-stage sequence [1, 17]. This process begins with the formation of a hydrated silica (SiO_2-gel) layer, followed by the precipitation of an amorphous calcium phosphate (ACP) film. This ACP layer then serves as a precursor, incorporating carbonate and hydroxyl ions from the solution before it finally crystallizes into a hydroxyl-carbonate apatite (HCA) layer. In stark contrast, our findings suggest a more direct and potentially more efficient pathway, where the pre-existing crystalline wollastonite lattice acts as a direct template for the heterogeneous nucleation of crystalline HA, seemingly bypassing the need for an intermediate amorphous precursor layer. This distinction is significant, as it suggests a higher degree of structural templating. On another front, sol-gel derived bioactive glasses represent a different kinetic extreme. Their intrinsically high nanoporosity and surface area lead to extremely rapid ion exchange and HA formation, but this often comes at the cost of significantly lower mechanical strength and structural integrity [18]. Our thermal processing approach offers a compelling middle ground, achieving robust mechanical properties through high-temperature sintering while precisely programming a tailored kinetic response at the surface, thus decoupling bulk mechanics from interfacial dynamics.

The final programmed biological outcome is a result of the complex interplay between HA layer formation and matrix degradation. The non-linear degradation profile (Figure 4) is the hallmark of a smart (4D) biomaterial. The initial high degradation rate makes room for the invasion of cells and vasculature, while the subsequent formation of a passivating, bioactive HA layer protects the underlying surface. This decreasing rate of deterioration prevents catastrophic failure and allows the implant to maintain its structural integrity as a stable scaffold for tissue regeneration. As a result, the material evolves from a synthetic ceramic into a biomimetic HA surface with the optimal chemistry and nanotopography to support osteoblast adhesion, proliferation, and differentiation [19, 20]. The therapeutic success of

this engineered interface hinges on these two synergistic events. The mature, crystalline HA layer provides the optimal physical substrate for bone-implant integration, while the regulated release of ions acts as a critical biological cue, modulating the immune response towards a healing M2 phenotype and orchestrating the cascade of cellular events leading to regeneration [21].

Beyond its direct effects on osteoblasts, the programmed ionic environment is critical for orchestrating the host immune response, a key determinant of long-term implant success. Upon implantation, the initial host response is dominated by macrophages, which can polarize into two main phenotypes: a pro-inflammatory M1 phenotype, which aims to destroy foreign pathogens, or a pro-regenerative M2 phenotype, which is involved in tissue repair and wound healing [22]. A persistent M1-dominated microenvironment leads to chronic inflammation and the formation of a non-integrating fibrous capsule, which is the primary failure mode for many implants. Therefore, a rapid and effective switch from an M1 to an M2 phenotype is essential for successful osteointegration. The controlled ionic dissolution products from the 1100°C A-W GC surface are hypothesized to play a crucial immunomodulatory role in facilitating this switch. Specifically, silicon ions have been demonstrated in numerous studies to promote the secretion of anti-inflammatory cytokines, such as IL-10 and TGF-β, and drive macrophage polarization towards the M2 lineage [23, 24]. By actively fostering a pro-regenerative milieu from the moment of implantation, the material is no longer a passive scaffold but an active participant that co-opts the host immune system to create a niche favorable for bone regeneration.

Essentially, this work provides a unified, biophysically based paradigm for the rational design of bioactive materials (Figure 5). We have moved beyond static compositional mimicry to demonstrate that the full kinetic pathway by which a material achieves its therapeutic function can be reliably programmed by carefully engineering its initial surface state. While this study provides a powerful kinetic blueprint using an acellular SBF model, future work will focus on validating this programmed response with in vitro osteoblast cultures to directly link the engineered interface to cellular outcomes.

These distinct but interconnected stages can be integrated into the unified kinetic model shown in Figure 5. This model provides a comprehensive blueprint that redefines the role of the material as a pre-programmed, dynamic system. The model illustrates how the initial design input, the engineered surface state controlled by sintering, directly dictates the entire cascade. It triggers the kinetic bio-interface transformation, including controlled ion exchange and templated nucleation, which in turn orchestrates the final therapeutic outcome of a mature, biomimetic surface and regulated degradation. This paradigm shifts the design of bioactive materials from static mimicry to the temporal engineering of a predictable biological response.

While this study provides a powerful kinetic blueprint for programming the bio-interface, it is essential to place our findings within a broader biological context. The use of an acellular SBF model is a necessary first step for isolating and quantifying the material-driven physicochemical cascade. However, the ultimate validation of bioactivity lies in the cellular response. In our previous work, we have already demonstrated that these engineered A-W GC surfaces exhibit excellent cytocompatibility with MC3T3-E1 pre-osteoblastic cells, as confirmed by MTT assays [10]. This foundational finding confirms that the materials are not cytotoxic and provide a suitable substrate for cell survival.

The present study builds directly upon that foundation by deconstructing the underlying kinetic mechanisms that govern the formation of the bioactive interface. The kinetic blueprint presented here provides the missing link, explaining why a surface engineered at 1100°C is primed for a superior biological outcome. The next logical step, therefore, is to move beyond simple viability and to directly correlate this programmed kinetic pathway with specific cell functions. Future research will focus on a time-resolved analysis of osteogenic differentiation, quantifying markers such as alkaline phosphatase (ALP) activity, collagen type I synthesis, and matrix mineralization (via Alizarin Red S staining) on these well-defined surfaces. Such studies will definitively link the engineered dissolution and reprecipitation kinetics to the temporal progression of osteogenesis, thereby completing the process-structure-property-performance relationship for this advanced biomaterial system.

5. Conclusion

Through this investigation, we have progressed from a static description of a bioactive ceramic to a dynamic, kinetic comprehension of its operation. For spray-pyrolyzed A-W GCs, we have successfully dissected the entire surface-interface-biological response cascade. The key finding of this work is that the entire spatiotemporal sequence of bio-interfacial processes is predictably programmed by the initial, sintering-induced phase composition, which is a master engineering variable.

We have developed a strong and accurate model for logical design by firmly establishing our analysis on the biophysical concepts of ion exchange, templated nucleation, and dissolution kinetics. We have shown that a high-temperature sintering-engineered wollastonite-rich surface not only exhibits higher bioactivity but also carries out a quicker and more effective kinetic pathway to produce a mature, biomimetic interface.

This work redefines the design of bioactive materials by offering a kinetic blueprint, so making a fundamental advancement in the field. Biomaterials engineering's future depends on carefully programming the kinetic pathway by which materials attain their therapeutic function over time, rather than just designing materials with desired endpoint attributes. The next generation of smart resorbable ceramics with biological responses preprogrammed for clinical applications and temporally regulated degradation can be developed using the fundamental ideas our model offers.

While this study provides a powerful kinetic blueprint using an acellular SBF model, future work will focus on validating this programmed response with in vitro osteoblast cultures to directly link the engineered interface to cellular outcomes.

6. Data Availability Statement

The data that support the findings of this study are available from the corresponding author upon reasonable request.

7. Funding Information

This research did not receive any specific grant from funding agencies in the public, commercial, or profit sectors.

8. Acknowledgments

For research support and access to analytical facilities, the authors are grateful to the National Taiwan University of Science and Technology's Department of Materials Science and Engineering. We also acknowledge the technical support from the university's Analytical Instrumentation Center under the direction of Prof. Shao-Ju Shih.

9. Declaration of Competing Interest

The authors have declared that no competing interests exist.

10. Ethical Compliance

This research did not involve human participants, human-derived materials, or animal studies. All research was conducted using synthetic materials and cellular SBF. Therefore, institutional ethical approval was not required.

11. Author Contributions

A.B.W. contributed to the implementation of the research, the formal analysis of the results, and the writing of the manuscript. S.-J.S. conceived the original idea, designed the study, and supervised the project.

References

[1] L. L. Hench, "Bioceramics: from concept to clinic," *Journal of the american ceramic society,* vol. 74, no. 7, pp. 1487-1510, 1991, doi: https://doi.org/10.1111/j.1151-2916.1991.tb07132.x.

[2] T. Kokubo, "Bioactive glass ceramics: properties and applications," *Biomaterials,* vol. 12, no. 2, pp. 155-163, 1991, doi: https://doi.org/10.1016/0142-9612(91)90194-F.

[3] T. Kokubo, S. Ito, S. Sakka, and T. Yamamuro, "Formation of a high-strength bioactive glass-ceramic in the system MgO-CaO-SiO2-P2O5," *Journal of Materials Science,* vol. 21, no. 2, pp. 536-540, 1986, doi: https://doi.org/10.1007/BF01145520.

[4] A. B. Workie and S.-J. Shih, "Mesoporous bioactive glasses: synthesis, characterization, and their medical applications," *Surface Review and Letters,* vol. 30, no. 04, p. 2330004, 2023, doi: https://doi.org/10.1142/S0218625X23300046.

[5] A. B. Workie and E. M. Sefene, "Ion-doped mesoporous bioactive glass: Preparation, characterization, and applications using the spray pyrolysis method," *RSC advances,* vol. 12, no. 3, pp. 1592-1603, 2022, doi: https://doi.org/10.1039/D1RA06113E.

[6] E. El-Meliegy and R. Van Noort, *Glasses and glass ceramics for medical applications*. Springer science & business media, 2011.

[7] A. B. Workie and S.-J. Shih, "A study of bioactive glass–ceramic's mechanical properties, apatite formation, and medical applications," *RSC advances,* vol. 12, no. 36, pp. 23143-23152, 2022, doi: https://doi.org/10.1039/D2RA03235J.

[8] K. Sugimoto, Y. Zhou, T. G. P. Galindo, R. Kimura, and M. Tagaya, "Investigation of surface layers on biological and synthetic hydroxyapatites based on bone mineralization process," *Biomimetics,* vol. 8, no. 2, p. 184, 2023, doi: https://doi.org/10.3390/BIOMIMETICS8020184.

[9] C. V. Putnis and A. Putnis, "A mechanism of ion exchange by interface-coupled dissolution-precipitation in the presence of an aqueous fluid," *Journal of Crystal Growth,* vol. 600, p. 126840, 2022, doi: https://doi.org/10.1016/J.JCRYSGRO.2022.126840.

[10] A. B. Workie, H. S. Ningsih, W.-L. Yeh, and S.-J. Shih, "An investigation of in vitro bioactivities and cytotoxicities of spray pyrolyzed apatite wollastonite glass-ceramics," *Crystals,* vol. 13, no. 7, p. 1049, 2023, doi: https://doi.org/10.3390/cryst13071049.

[11] A. B. Workie, H. S. Ningsih, and S.-J. Shih, "An comprehensive review on the spray pyrolysis technique: Historical context, operational factors, classifications, and product applications," *Journal of Analytical and Applied Pyrolysis,* vol. 170, p. 105915, 2023, doi: https://doi.org/10.1016/j.jaap.2023.105915.

[12] T. Kokubo and S. Yamaguchi, "Simulated body fluid and the novel bioactive materials derived from it," *Journal of Biomedical Materials Research Part A,* vol. 107, no. 5, pp. 968-977, 2019, doi: https://doi.org/10.1002/jbm.a.36620.

[13] W. Zhang *et al.*, "Studies on anion exchange membrane and interface properties by electrochemical impedance spectroscopy: The Role of pH," *Membranes,* vol. 11, no. 10, p. 771, 2021, doi: https://doi.org/10.3390/membranes11100771.

[14] D. I. Viswanath, H.-C. Liu, D. P. Huston, C. Y. X. Chua, and A. Grattoni, "Emerging biomaterial-based strategies for personalized therapeutic in situ cancer vaccines," *Biomaterials,* vol. 280, p. 121297, 2022, doi: https://doi.org/10.1016/j.biomaterials.2021.121297.

[15] R. Ahmad and J. E. Dalziel, "G protein-coupled receptors in taste physiology and pharmacology," *Frontiers in pharmacology,* vol. 11, p. 587664, 2020, doi: https://doi.org/10.3389/fphar.2020.587664.

[16] C. Magnusson and M. Ransjö, "Orthosilicic acid inhibits human osteoclast differentiation and bone resorption," *PLoS One,* vol. 19, no. 10, p. e0312169, 2024, doi: https://doi.org/10.1371/journal.pone.0312169.

[17] A. Obata, S. Lee, and T. Kasuga, "Bioactive glass materials for tissue regeneration," *Journal of the Ceramic Society of Japan,* vol. 130, no. 8, pp. 595-604, 2022, doi: https://doi.org/10.2109/jcersj2.22054.

[18] M. Chen, Y. Wang, P. Yuan, L. Wang, X. Li, and B. Lei, "Multifunctional bioactive glass nanoparticles: surface–interface decoration and biomedical applications," *Regenerative Biomaterials,* vol. 11, p. rbae110, 2024, doi: https://doi.org/10.1093/rb/rbae110.

[19] M. Montazerian and E. Dutra Zanotto, "History and trends of bioactive glass-ceramics," *Journal of Biomedical Materials Research Part A,* vol. 104, no. 5, pp. 1231-1249, 2016, doi: https://doi.org/10.1002/jbm.a.35639.

[20] J. Qian *et al.*, "Osteogenic and angiogenic bioactive collagen entrapped calcium/zinc phosphates coating on biodegradable Zn for orthopedic implant applications," *Biomaterials Advances,* vol. 136, p. 212792, 2022, doi: https://doi.org/10.1016/j.bioadv.2022.212792.

[21] G. Rafikova *et al.*, "Interaction of ceramic implant materials with immune system," *International Journal of Molecular Sciences,* vol. 24, no. 4, p. 4200, 2023, doi: https://doi.org/10.3390/IJMS24044200.

[22] M. H. Abdelaziz *et al.*, "Alternatively activated macrophages; a double-edged sword in allergic asthma," *Journal of translational medicine,* vol. 18, no. 1, p. 58, 2020, doi: https://doi.org/10.1186/s12967-020-02251-w.

[23] Y.-H. Lin, C.-Y. Chen, K.-H. Chen, T.-Y. Kuo, T.-L. Lin, and M.-Y. Shie, "Lithium-doped calcium silicate cement regulates the immune microenvironment and promotes M2 macrophage polarization for enhancing bone regeneration," *Journal of Biological Engineering,* vol. 19, no. 1, p. 3, 2025, doi: https://doi.org/10.1186/s13036-024-00467-8.

[24] M. Vallet-Regí, M. Colilla, I. Izquierdo-Barba, C. Vitale-Brovarone, and S. Fiorilli, "Achievements in mesoporous bioactive glasses for biomedical applications," *Pharmaceutics,* vol. 14, no. 12, p. 2636, 2022, doi: https://doi.org/10.3390/pharmaceutics14122636.